# Supporting information

# Core-shell Ag@Polypyrrole for Synchronous Pre-enrichment and Immobilization of Iodine ($I^-$, $IO_3^-$) from Liquid Radioactive Wastes

Qian Zhao[a,b,c,d], Ruixi Liu[a,b,c,d], Zeru Wang[a,b,c,d], Guangyuan Chen[a,b,c,d],Tao Duan[a,b,c,d], Lin Zhu[a,b,c,d,*]

[a] National Co-Innovation Center for Nuclear Waste Disposal and Environmental Safety, Southwest University of Science and Technology, Mianyang 621010, China

[b] Tianfu Institute of Research and Innovation, Southwest University of Science and Technology, Chengdu 610299, China

[c] State Key Laboratory of Environment-Friendly Energy Materials, Southwest University of Science and Technology, Mianyang 621010, China

[d] School of Environment and Resource, Southwest University of Science and Technology, Mianyang 621010, China

*Corresponding Authors Email: zhulin@swust.edu.cn (Lin Zhu)

**S1. Study of stability**

In order to determine the acid-base stability of the adsorbent, the leaching rate of Ag@PPy was measured. Typically, 5 mg sample is added to a 20 mL aqueous solution. The pH was adjusted to 3-11 with NaOH and $HNO_3$ solutions. The concentration of Ag in the aqueous solution was determined by ICP-MS.

**S2. $I^-/IO_3^-$ adsorption**

For safety concerns, we used the nonradioactive iodine isotope to monitor the behavior of $^{131}I$ and $^{129}I$. A fixed amount of adsorbent was added to a series of KI and $KIO_3$ solutions at concentrations of 10 to 500 ppm. The resulting mixture was stirred for a desired contact time by magnetic stirrer. Afterward, the supernatant was collected by fltering the mixture with a 0.22 μm nylon membrane filter and measured by ultraviolet spectrophotometer (UV−vis) at 226 nm to determine the remaining $I^-$ anions in the solutions. In addition, the $IO_3^-$ was determined by the absorbance of triiodide ($I_3^-$) at 350 nm. Typically, $IO_3^-$ was converted to $I_3^-$, which owns characteristic peaks in the UV absorption spectrum, by sequentially mixing 1 mL of 1 mL of 0.1 M $H_3PO_4$, 1 mL of 2% KI and 2 mL of $IO_3^-$ sample.

**S3. Adsorbent dosage and effect of pH experiments**

Experimental studies of adsorbent dosage were carried out at room temperature with varying amounts (0.1-0.8 g/L) of Ag@PPy using 20mL of initial concentration of iodide at 200 mg/L at pH 7.0. For the effect of pH experiments, the initial concentration of iodide and iodate was 200 mg/L. The pH was adjusted to 3-11 with NaOH and $HNO_3$ solutions. The concentrations of iodine in aqueous solution were determined by UV−vis.

**S4. Adsorption Kinetics**

Adsorption kinetics were used to analyze the adsorption rate and elucidate the potential rate-controlling mechanism of the adsorption process. To design the appropriate adsorption systems, two well-known kinetics models, pseudo-first-order and pseudo-second-order rate equations are analyzed. The pseudo-first-order and pseudo-second-order equations can be expressed as follows:

$$\ln(q_e - q_t) = \ln q_e - k_1 t \quad (1)$$

$$\frac{t}{q_t} = \frac{1}{k_2 q_e^2} + \frac{t}{q_e} \tag{2}$$

where $t$ is the contact time (h), $q_t$ and $q_e$ are the amounts of $I^-/IO_3^-$ absorbed at time $t$ and at equilibrium (mg/g), respectively, and $k_1$ (1/h) and $k_2$ (g/mg h) are the rate constant. The results are listed in **Table S3**.

**S5. The sorption data fitting by isotherm models**

The Langmuir model assumes that the monolayer sorption occurs on a homogeneous surface and every adsorption sites is equivalent and identical; whereas the Freundlich isotherm is an empirical equation assuming that multilayer adsorption process occurs on the heterogeneous surface. Their linear equation can be expressed as followed:

$$\ln q_e = \ln K_F + n \ln C_e \tag{3}$$

$$\frac{C_e}{q_e} = \frac{C_e}{q_m} + \frac{1}{q_m K_L} \tag{4}$$

Where $C_e$ and $q_e$ are the concentration of adsorbate (mg/L) and the adsorption capacity of the adsorbent (mg/g) at equilibrium, respectively. $q_m$ is the maximum sorption capacity (mg/g) and $K_L$ is the Langmuir adsorption constant (L/mg), which characterizes the affinity of the adsorbate with the adsorbent. Where $K_F$ and $n$ are the Freundlich constants related to the sorption capacity and the sorption intensity, respectively. **Table S4** shows the fitting results from the Langmuir and Freundlich equations.

The distribution coefficient $K_d$ was calculated using the following equation:

$$K_d = \frac{C_0 - C_e}{C_e} \times \frac{V}{m} \tag{5}$$

where $C_0$ and $C_e$ represent the iodide or iodate concentrations in aqueous solution before and after sorption equilibrium, respectively. $V$ and $m$ are the volume of aqueous solution and the weight of dry sorbent. Generally, the higher the $K_d$ (mL/g) value, the better is the sorption properties.[1]

**S6. Simulated wastewater experiment**

The solutions were prepared by adding an appropriate amount of potassium iodide (KI)

or potassium iodate ($KIO_3$) to the simulated groundwater to obtain 1.0 mg/L of iodine. The simulated artificial groundwater was prepared by adding reagents to deionized water in the order determined in **Table S7**. Once the chemicals have dissolved, excess calcium carbonate ($CaCO_3$) was added to regenerate the carbonate-saturated Hanford Site groundwater, and the solution was stirred. After approximately one week, the solution was filtered using a 0.22 μm filter to remove excess $CaCO_3$. The pH of the SGW previously containing potassium iodide and potassium iodate was 8.20 and 8.18, respectively.

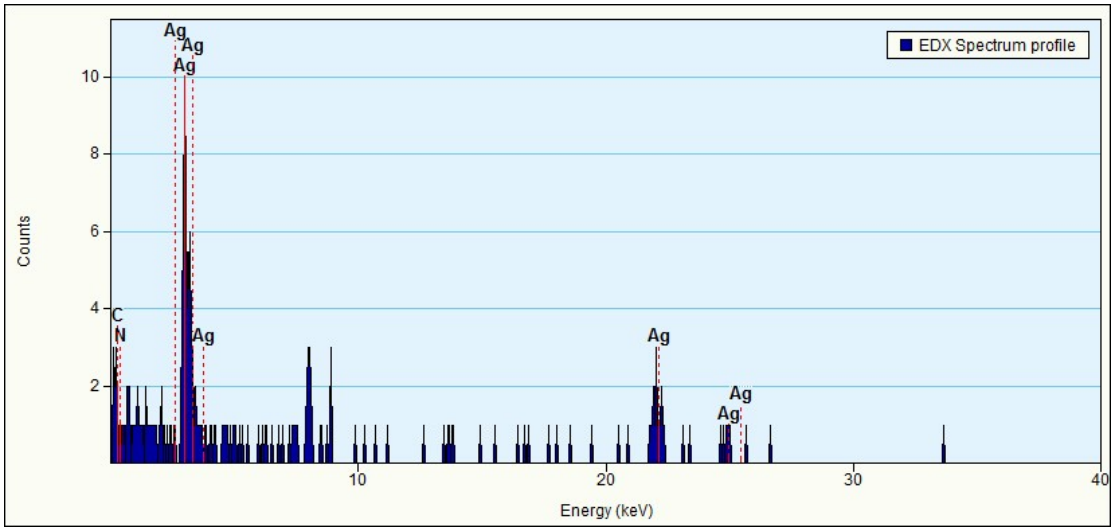


**Figure S1.** The EDX spectra of Ag@PPy.

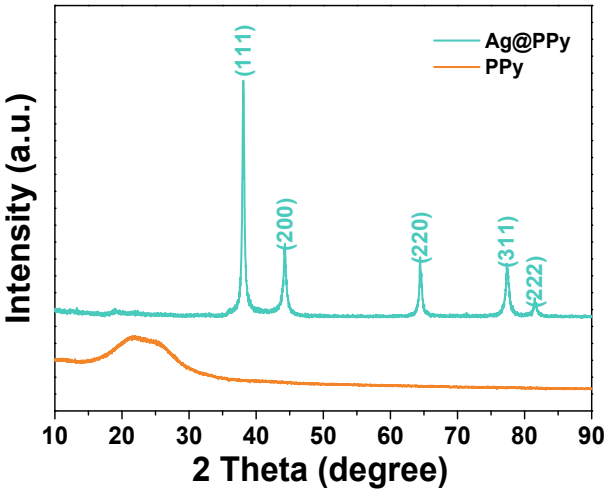


**Figure S2.** XRD patterns of PPy and Ag@PPy.

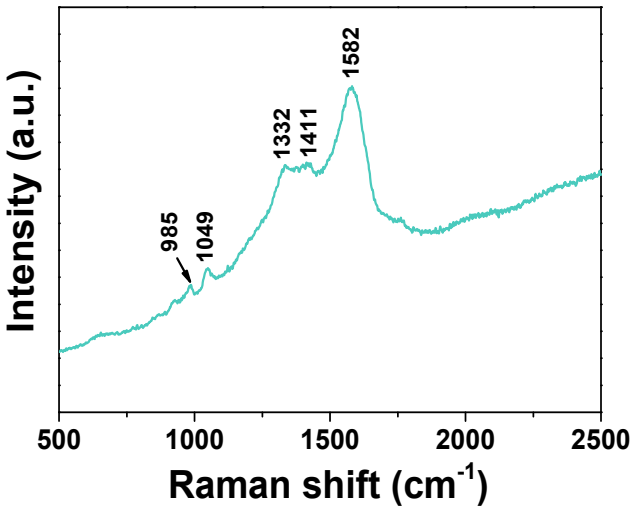


**Figure S3.** Raman spectra of Ag@PPy.

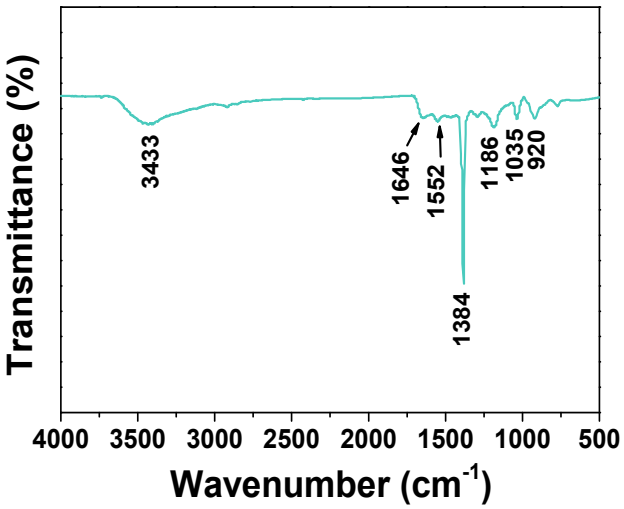


**Figure S4.** FTIR spectroscopy of Ag@PPy.

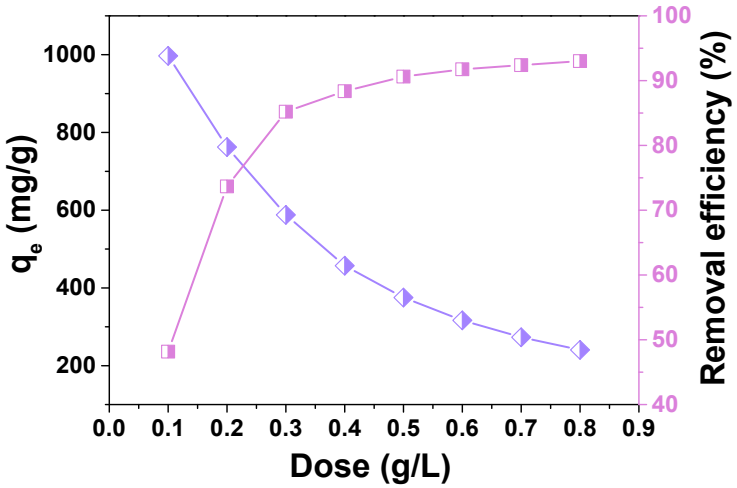


**Figure S5.** Effect of dosage on adsorption of $I^-$ by Ag@PPy. ($I^-$: 200 mg/L, pH: ~7.0, contact time: 48h)

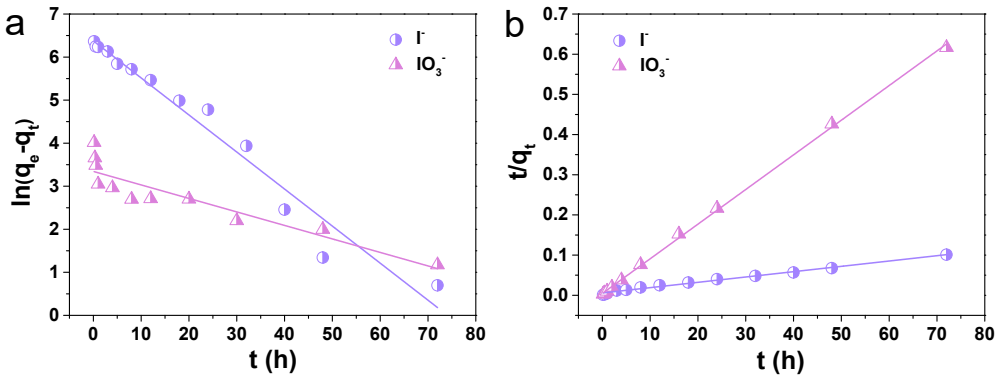


**Figure S6.** (a) Pseudo-first-order kinetics and (b) pseudo-second-order kinetics models for $I^-$ and $IO_3^-$ adsorption on Ag@PPy.

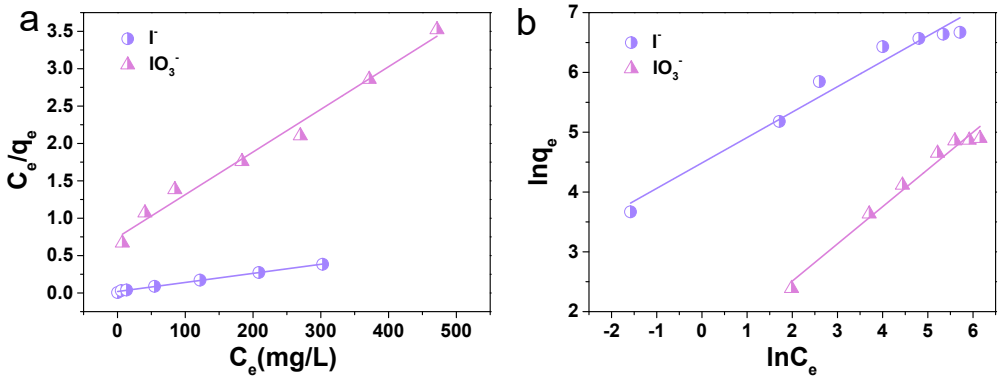


**Figure S7.** (a) Langmuir and (b) Freundlich isotherm models for $I^-$ and $IO_3^-$ adsorption on Ag@PPy.

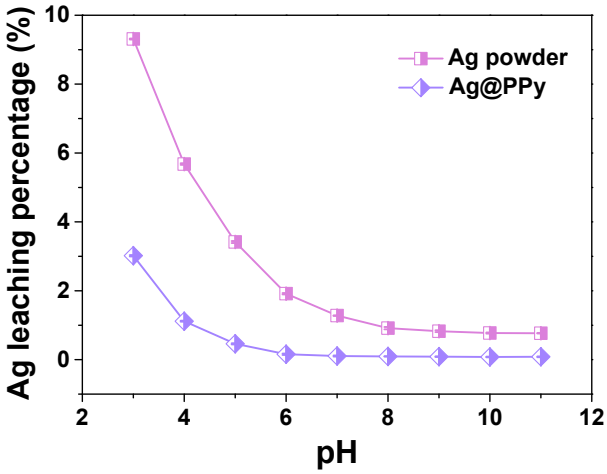


**Figure S8.** The Ag leaching percentage of Ag powder and Ag@PPy at pH = 3–11.

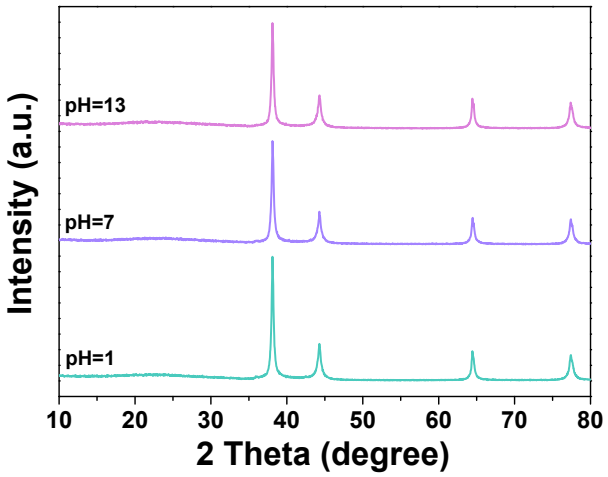


**Figure S9**. XRD patterns of Ag@PPy after immersed in different pH solutions.

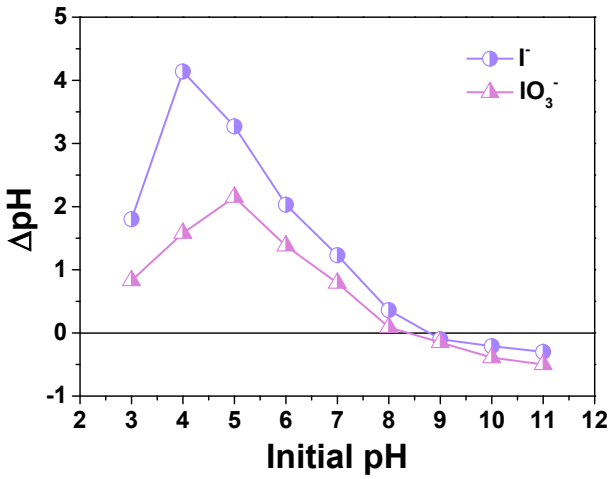


**Figure S10.** The pH after $I^-$ and $IO_3^-$ sorption.

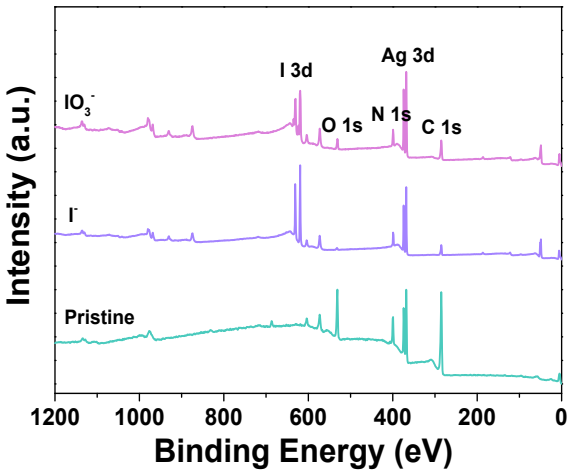


**Figure S11.** XPS spectra of Ag@PPy after $I^-$ and $IO_3^-$ adsorption.

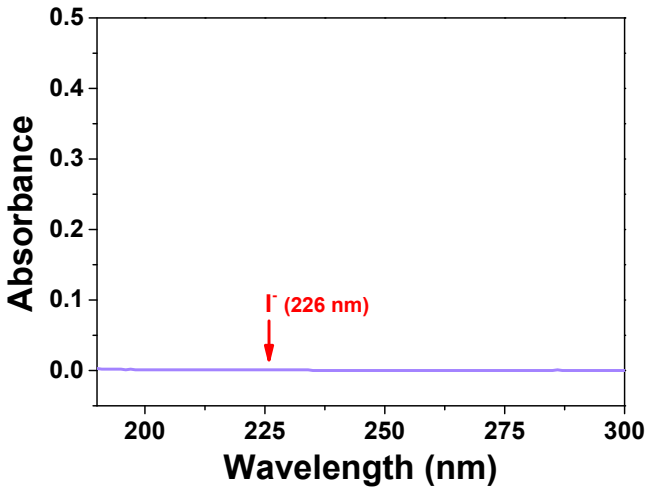


**Figure S12.** UV−vis absorption spectra of $I^-$ during the $IO_3^-$ adsorption.

**Table S1.** Comparison of pseudo-first-order kinetics and pseudo-second-order kinetics and experimental and calculated $q_e$ values.

| sample | $q_e$ (mg/g) | Pseudo-first-order | | | Pseudo-second-order | | |
|---|---|---|---|---|---|---|---|
| | | $k_1$ (1/h) | $q_e$ (mg/g) | $R^2$ | $k_2$ (g/mg h) | $q_e$ (mg/g) | $R^2$ |
| $I^-$ | 703.3 | $8.61\times10^{-2}$ | 587.68 | 0.959 | $3.09\times10^{-4}$ | 751.88 | 0.991 |
| $IO_3^-$ | 100.7 | $3.14\times10^{-2}$ | 28.33 | 0.824 | $1.64\times10^{-2}$ | 116.01 | 0.999 |

**Table S2.** Fitting results of the isothermal sorption according to the Langmuir and Freundlich equations.

| sample | Langmuir constant | | | Freundlich constant | | |
|---|---|---|---|---|---|---|
| | $q_m$(mg/g) | $K_L$ (L/mg) | $R^2$ | $n$ | $K_F$ (mg/g) | $R^2$ |
| $I^-$ | 826.45 | $6.4\times10^{-2}$ | 0.997 | 0.425 | 88.80 | 0.964 |
| $IO_3^-$ | 175.13 | $7.68\times10^{-3}$ | 0.982 | 0.622 | 3.55 | 0.976 |

**Table S3.** Iodide adsorption in various materials reported previously in the literature.

| Adsorbent | pH | Uptake (mg/g) | $K_d$ (mL/g) | Reference |
|---|---|---|---|---|
| Modified zeolite | 7.0 | 4.02 | - | 2 |
| Surfactant-modified bentonite | 8.0 | 70.0 | $4.2\times10^3$ | 3 |
| Purolite A530E resin | 7.0 | 275.16 | - | 4 |
| Microrosette-like δ-$Bi_2O_3$ | 6.5 | 182.9 | - | 5 |
| δ-$Bi_2O_3$@PES | 7.0 | 95.4 | - | 6 |
| NiAl LDH | 5.8-6.4 | 266.7 | - | 7 |
| CoAl LDH | 5.8-6.4 | 212.09 | - | 7 |
| AgCl@calcium alginate | 6.0 | 139.7 | - | 8 |
| MIL-101(Cr)-$SO_3Ag$ | 7.5 | 244.2 | - | 9 |

| | | | | |
|---|---|---|---|---|
| $Ag_2O$-SNF | 7.0 | 292.1 | - | 10 |
| Ag@$Cu_2O$ | 7.0 | 25.4 | - | 11 |
| A-Ag-15 | 7.0 | 251.47 | - | 12 |
| Ag@activated carbon | 5.0 | 340.6 | - | 13 |
| $Ag_2O$-T3NL | 7.0 | 431.8 | - | 14 |
| $Ag_2O$-T3NT | 7.0 | 571.5 | - | 14 |
| Ag-$Ag_2O$-CSs | 2.2 | 374.9 | - | 15 |
| Ag-MSHC-6 | 8.0 | 771.6 | - | 16 |
| Ag-C | 7.0 | - | $6.2\times10^5$ | 17 |
| Argentite | 7.0 | - | $3.7\times10^5$ | 17 |
| Ag-Z | 7.0 | | $9.1\times10^4$ | 17 |
| Ag-GAC | 11.12±0.01 | - | > 4423 | 18 |
| AgAero | 7.0 | - | $1.5\times10^4$ | 19 |
| Field soil | - | - | 7500 | 20 |
| Paddy soil | - | - | 560 | 20 |
| Sandy soil | - | - | 35 | 20 |
| $Cu_2O$@CH | 3.0 | 416.5 | $4.23\times10^3$ | 21 |
| **Ag@PPy** | **6.5-7.0** | **788.7** | **$3.90\times10^5$** | **This work** |

**Table S4.** Iodate adsorption in various materials reported previously in the literature.

| Adsorbent | pH | Uptake (mg/g) | $K_d$ (mL/g) | Reference |
|---|---|---|---|---|
| PB-LDH | - | 91 | - | 22 |
| $Mg_2$-Al-$NO_3$ LDH | - | 149.528 | - | 23 |
| NiAl LDH | 5.8-6.4 | 395.5 | 2126 | 7 |
| CoAl LDH | 5.8-6.4 | 378 | 1692 | 7 |
| DNTD | 5.6 | 1.31 | - | 24 |
| Activated Carbon F400 | 4.0 | 40.25 | - | 25 |
| MOF-808 | - | 233 | - | 26 |
| Purolite A530E resin | 7.0 | 53.34 | - | 4 |

| | | | | |
|---|---|---|---|---|
| Pomelo peel | - | 6.81 | - | 27 |
| δ-$Bi_2O_3$@PES | 7.0 | 170.6 | - | 6 |
| Corn stalk | 7±0.3 | 0.534 | 49.73 | 28 |
| Ag-GAC | 11.16±0.07 | - | 612±25 | 18 |
| BIN | 7.0-8.0 | - | $2.14\times10^7$ | 29 |
| FeH | 7.0-8.0 | - | $8.39\times10^4$ | 29 |
| $CeO_2$ | 7.0-8.0 | - | 45 | 29 |
| FeA | 7.0-8.0 | - | 14 | 29 |
| CHM-20 | 7.0-8.0 | - | $1.27\times10^6$ | 29 |
| ASM-10-HP | 7.0-8.0 | - | $8.57\times10^5$ | 29 |
| Bismuth (oxy)hydroxide | 7.96 | - | $2.02\times10^5$ | 30 |
| Sb-doped $ZrO_2$ | 6.0 | 560-612.5 | $5.0\times10^4$ | 31 |
| HFO | 7.3-7.6 | - | 1220.8 | 32 |
| Magnetite | 7.0-7.5 | - | 30.3 | 32 |
| Hematite | 7.3-7.5 | - | 12.5 | 32 |
| Goethite | 7.1-7.3 | - | 125.8 | 32 |
| $Cu_2O$@CH | 6.0 | 313.4 | $5.33\times10^2$ | 21 |
| **Ag@PPy** | **6.0-7.0** | **133.9** | **$2.30\times10^5$** | **This work** |

**Table S5.** Total iodine concentrations in different contaminated waters and wastewaters.

| Region | Iodine concentration | Reference |
|---|---|---|
| Drinking waters from Bryansk | 0.068-50.14 μg/L | Elena Korobova et al.[33] |
| Groundwater in the wetlands | ~59.9 Bq/L | Daniel I. Kaplan et al.[34] |
| Groundwater system at Datong basin, China | 3.31-1890 μg/L | Junxia Li et al.[35] |
| River waters | ~0.7-212 μg/L | Sungwook Choung et al.[36] |
| Hanford Site | <100 μg/L | Sarah A. Saslow et al.[37] |
| Savannah River Site | 4.0-10.7 μg/L | Jean E. Moran et al.[38] |

**Table S6.** Synthetic Hanford Groundwater (SGW)[30]

| Constituent | Concentration (mg/L) |
|---|---|
| $H_2SiO_3$*$nH_2O$, silicic acid | 15.3 |
| KCl, potassium chloride | 8.20 |
| $MgCO_3$, magnesium carbonate | 13.0 |
| NaCl, sodium chloride | 15.0 |
| $CaSO_4$, calcium sulfate | 67.0 |
| $CaCO_3$, calcium carbonate | 150 |

**Table S7**. Uptake of $I^-$ and $IO_3^-$ onto Ag@PPy Material by simulated Hanford wastewater experiment. (Initial concentration:1 mg/L, Contact time: 48 h)

| m/V（g/L） | $I^-$ | | | $IO_3^-$ | | |
|---|---|---|---|---|---|---|
| | final (mg/L) | removal (%) | $K_d$ (mL/g) | final (mg/L) | removal (%) | $K_d$ (mL/g) |
| **0.25** | 0.89 | 10.71 | $4.80\times10^2$ | 0.96 | 3.94 | $1.64\times10^2$ |
| **0.5** | 0.58 | 41.79 | $1.44\times10^3$ | 0.95 | 5.18 | $1.09\times10^2$ |
| **1** | 0.36 | 64.29 | $1.80\times10^3$ | 0.93 | 7.33 | $7.91\times10$ |
| **2** | 0.19 | 81.43 | $2.19\times10^3$ | 0.86 | 14.09 | $8.20\times10$ |
| **5** | 0.14 | 86.43 | $1.27\times10^3$ | 0.47 | 52.87 | $2.24\times10^2$ |

**References**


1. G. E. Fryxell, Y. Lin, S. Fiskum, J. C. Birnbaum and S. Kelly, Actinide Sequestration Using Self-Assembled Monolayers on Mesoporous Supports, *Environ. Sci. Technol.*, 2005, **39**, 1324-1331.
2. J. Warchol, P. Misaelides, R. Petrus and D. Zamboulis, Preparation and application of organo-modified zeolitic material in the removal of chromates and iodides, *J. Hazard. Mater.*, 2006, **137**, 1410-1416.
3. S. Choung, M. Kim, J. S. Yang, M. G. Kim and W. Um, Effects of Radiation

and Temperature on Iodide Sorption by Surfactant-Modified Bentonite, *Environ. Sci. Technol.*, 2014, **48**, 9684-9691.

4. Y. Zhao, J. Li, L. Chen, Q. Guo, L. Li, Z. Chai and S. Wang, Efficient removal of iodide/iodate from aqueous solutions by Purolite A530E resin, *J. Radioanal. Nucl. Chem.*, 2023, **332**, 1193-1202.
5. L. Liu, W. Liu, X. Zhao, D. Chen, R. Cai, W. Yang, S. Komarneni and D. Yang, Selective capture of iodide from solutions by microrosette-like δ-$Bi_2O_3$, *ACS Appl. Mater. Interfaces*, 2014, **6**, 16082-16090.
6. Q. Zhao, G. Chen, Z. Wang, M. Jiang, J. Lin, L. Zhang, L. Zhu and T. Duan, Efficient removal and immobilization of radioactive iodide and iodate from aqueous solutions by bismuth-based composite beads, *Chem. Eng. J.*, 2021, **426**, 131629.
7. J. Kang, F. Cintron-Colon, H. Kim, J. Kim, T. Varga, Y. Du, O. Qafoku, W. Um and T. G. Levitskaia, Removal of iodine ($I^-$ and $IO_3^-$) from aqueous solutions using CoAl and NiAl layered double hydroxides, *Chem. Eng. J.*, 2022, **430**, 132788.
8. H. Zhang, X. Gao, T. Guo, Q. Li, H. Liu, X. Ye, M. Guo and Z. Wu, Adsorption of iodide ions on a calcium alginate-silver chloride composite adsorbent, *Colloids Surf. A Physicochem. Eng. Aspects*, 2011, **386**, 166-171.
9. X. Zhao, X. Han, Z. Li, H. Huang, D. Liu and C. Zhong, Enhanced removal of iodide from water induced by a metal-incorporated porous metal-organic framework, *Appl. Surf. Sci.*, 2015, **351**, 760-764.
10. W. Mu, Q. Yu, X. Li, H. Wei and Y. Jian, Niobate nanofibers for simultaneous adsorptive removal of radioactive strontium and iodine from aqueous solution, *J. Alloys Compd.*, 2017, **693**, 550-557.
11. P. Mao, Y. Liu, Y. Jiao, S. Chen and Y. Yang, Enhanced uptake of iodide on Ag@$Cu_2O$ nanoparticles, *Chemosphere*, 2016, **164**, 396-403.
12. M. Sanchez-Polo, J. Rivera-Utrilla, E. Salhi and U. V. Gunten, Ag-doped carbon aerogels for removing halide ions in water treatment, *Water Res.*, 2007, **41**, 1031-1037.

13. J. S. Hoskins, T. Karanfil and S. M. Serkiz, Removal and Sequestration of Iodide Using Silver-Impregnated Activated Carbon, *Environ. Sci. Technol.*, 2002, **36**, 784-789.

14. A. Bo, S. Sarina, Z. Zheng, D. Yang, H. Liu and H. Zhu, Removal of radioactive iodine from water using $Ag_2O$ grafted titanate nanolamina as efficient adsorbent, *J. Hazard. Mater.*, 2013, **246-247**, 199-205.

15. F. Yu, Y. Chen, Y. Wang, C. Liu and W. Ma, Enhanced removal of iodide from aqueous solution by ozonation and subsequent adsorption on Ag-$Ag_2O$ modified on Carbon Spheres, *Appl. Surf. Sci.*, 2018, **427**, 753-762.

16. H. Li, Y. Li, B. Li, D. Liu and Y. Zhou, Highly selective anchoring silver nanoclusters on MOF/SOF heterostructured framework for efficient adsorption of radioactive iodine from aqueous solution, *Chemosphere*, 2020, **252**, 126448.

17. R. M. Asmussen, J. J. Neeway, A. R. Lawter, A. Wilson and N. P. Qafoku, Silver-based getters for $^{129}I$ removal from low-activity waste, *Radiochim. Acta*, 2016, **104**, 905-913.

18. D. Li, D. I. Kaplan, K. A. Price, J. C. Seaman, K. Roberts, C. Xu, P. Lin, W. Xing, K. Schwehr and P. H. Santschi, Iodine immobilization by silver-impregnated granular activated carbon in cementitious systems, *J. Environ. Radioact.*, 2019, **208-209**, 106017.

19. R. M. Asmussen, J. Matyas, N. P. Qafoku and A. A. Kruger, Silver-functionalized silica aerogels and their application in the removal of iodine from aqueous environments, *J. Hazard. Mater.*, 2019, **379**, 119364.

20. Y. Muramatsu, S. Uchida, P. Sriyotha and K. Sriyotha, Some considerations on the sorption and desorption phenomena of iodide and iodate on soil, *Water Air Soil Poll.*, 1990, **49**, 125-138.

21. C. Yan, J. Li, C. Tan, G. Chen, Q. Zhao, Y. Chen, P. He, Y. Luo, T. Duan, J. Lei and L. Zhu, Cuprous Oxide-Based Cationic Hydrogel by the Integration of Enrichment and Immobilization of Radioiodine ($I^-$, $IO_3^-$) in Aqueous Solution, *ACS Appl. Mater. Interfaces*, 2023, **15**, 28135-28148.

22. J. Kim, J. Kang and W. Um, Simultaneous removal of cesium and iodate using prussian blue functionalized CoCr layered double hydroxide (PB-LDH), *J. Environ. Chem. Eng.*, 2022, **10**, 107477.

23. D. Zhang, X. Y. Liu, H. T. Zhao, L. Yang, T. Lu and M. Q. Jin, Application of hydrotalcite in soil immobilization of iodate ($IO_3^-$), *RSC Adv.*, 2018, **8**, 21084-21091.

24. P. Liu, T. Chen and J.-g. Zheng, Removal of iodate from aqueous solution using diatomite/nano titanium dioxide composite as adsorbent, *J. Radioanal. Nucl. Chem.*, 2020, **324**, 1179-1188.

25. R. Mahmudov and C. P. Huang, Selective adsorption of oxyanions on activated carbon exemplified by Filtrasorb 400 (F400), *Sep. Purif. Technol.*, 2011, **77**, 294-300.

26. C. Copeman, H. A. Bicalho, M. W. Terban, D. Troya, M. Etter, P. L. Frattini, D. M. Wells and A. J. Howarth, Adsorptive Removal of Iodate Oxyanions from Water using a Zr-based Metal-Organic Framework, *Chem. Commun.*, 2023, **59**, 3071-3074.

27. T. Da and T. Chen, Optimization of experimental factors on iodate adsorption: a case study of pomelo peel, *J. Radioanal. Nucl. Chem.*, 2020, **326**, 511-523.

28. K. Zhang and T. Chen, Dried powder of corn stalk as a potential biosorbent for the removal of iodate from aqueous solution, *J. Environ.Radioactiv.*, 2018, **190-191**, 73-80.

29. E. A. Cordova, V. Garayburu-Caruso, C. I. Pearce, K. J. Cantrell, J. W. Morad, E. C. Gillispie, B. J. Riley, F. C. Colon, T. G. Levitskaia, S. A. Saslow, O. Qafoku, C. T. Resch, M. J. Rigali, J. E. Szecsody, S. M. Heald, M. Balasubramanian, P. Meyers and V. L. Freedman, Hybrid Sorbents for $^{129}I$ Capture from Contaminated Groundwater, *ACS Appl. Mater. Interfaces*, 2020, **12**, 26113-26126.

30. C. I. Pearce, E. A. Cordova, W. L. Garcia, S. A. Saslow, K. J. Cantrell, J. W. Morad, O. Qafoku, J. Matyas, A. E. Plymale, S. Chatterjee, J. Kang, F. C. Colon, T. G. Levitskaia, M. J. Rigali, J. E. Szecsody, S. M. Heald, M.

Balasubramanian, S. Wang, D. T. Sun, W. L. Queen, R. Bontchev, R. C. Moore and V. L. Freedman, Evaluation of materials for iodine and technetium immobilization through sorption and redox-driven processes, *Sci. Total Environ.*, 2020, **716**, 136167.

31. V. Suorsa, M. Otaki, J. Virkanen and R. Koivula, Pure and Sb-doped $ZrO_2$ for removal of $IO_3^-$ from radioactive waste solutions, *Int. J. Environ. Sci. Technol.*, 2021, **19**, 5155-5166.
32. G. Wang, N. P. Qafoku, J. E. Szecsody, C. E. Strickland, C. F. Brown and V. L. Freedman, Time-Dependent Iodate and Iodide Adsorption to Fe Oxides, *ACS Earth and Space Chem.*, 2019, **3**, 2415-2420.
33. E. Korobova, L. Kolmykova, B. Ryzhenko, E. Makarova, V. Shkinev, E. Cherkasova, N. Korsakova, I. Gromyak, V. Berezkin and V. Baranchukov, Distribution and speciation of iodine in drinking waters from geochemically different areas of Bryansk region contaminated after the Chernobyl accident in relation to health and remediation aspects, *J. Geochem. Explor.*, 2018, **184**, 311-317.
34. D. I. Kaplan, S. Zhang, K. A. Roberts, K. Schwehr, C. Xu, D. Creeley, Y. F. Ho, H. P. Li, C. M. Yeager and P. H. Santschi, Radioiodine concentrated in a wetland, *J. Environ. Radioact.*, 2014, **131**, 57-61.
35. J. Li, Y. Wang, X. Xie, L. Zhang and W. Guo, Hydrogeochemistry of high iodine groundwater: a case study at the Datong Basin, northern China, *Environ. Sci.: Process Impacts*, 2013, **15**, 848-859.
36. S. Choung, W. Um, M. Kim and M. G. Kim, Uptake mechanism for iodine species to black carbon, *Environ. Sci. Technol.*, 2013, **47**, 10349-10355.
37. S. A. Saslow, S. N. Kerisit, T. Varga, K. C. Johnson, N. M. Avalos, A. R. Lawter and N. P. Qafoku, Chromate Effect on Iodate Incorporation into Calcite, *ACS Earth Space Chem.*, 2019, **3**, 1624-1630.
38. J. E. Moran, S. D. Oktay and P. H. Santschi, Sources of iodine and iodine 129 in rivers, *Water Resour. Res.*, 2002, **38**, 24-21-24-10.